High Resolution Optical/Near-Infrared Imaging of Cool Ultraluminous Infrared Galaxies

Jason A. Surace
Infrared Processing and Analysis Center, MS 100–22, California Institute of Technology, Jet Propulsion Laboratory, Pasadena, CA 91125
and
University of Hawaii, Institute for Astronomy, 2680 Woodlawn Dr., Honolulu, HI, 96822
Electronic mail: jason@ipac.caltech.edu

D. B. Sanders
University of Hawaii, Institute for Astronomy, 2680 Woodlawn Dr., Honolulu, HI, 96822
Electronic mail: sanders@ifa.hawaii.edu
and

A.S. Evans
Dept. of Physics and Astronomy, SUNY, Stony Brook, NY 11794-3800
and
California Institute of Technology 105-24, Pasadena, CA 91125
Electronic mail: aevans@vulcan.ess.sunysb.edu

Accepted for Publication in *The Astrophysical Journal*

ABSTRACT

We present high spatial resolution (FWHM $\approx$ 0.3–0.8″) BIHK′-band imaging of a sample of ultraluminous infrared galaxies ($L_{ir} > 10^{12}\ L_{\odot}$; ULIGs) with "cool" mid-infrared colors ($f_{25\mu m}/f_{60\mu m} < 0.2$) which select against AGN-like systems and which form a complementary sample to the "warm" ULIGs of Surace et al. (1998). We find that all of the cool ULIGs are either advanced mergers or are pre-mergers with evidence for still- separate nuclei with separations greater than 600 pc. Extended tidal features such as tails and loops as well as clustered star formation are observed in most systems. This extended tidal structure suggests a common progenitor geometry for most of the ULIGs: a plunging disk collision where the disks are highly inclined with respect to each other. The underlying host galaxies have H-band luminosities of 1–2.5 L^*, very similar to that found in the "warm" ULIGs. The nuclear regions of these galaxies have morphologies and colors characteristic of a recent burst of star formation mixed

with hot dust and mildly extinguished by A_V=2–5 magnitudes; only in one case (IRAS 22491−1808) is there evidence for a compact emission region with colors similar to an extinguished QSO. Most of the observed star-forming knots appear to have very young (10 Myr) ages based on their optical/near-infrared colors. These star-forming knots are insufficiently luminous to typically provide more than 10% of the high bolometric luminosity of the systems.

Subject headings: infrared: galaxies—galaxies: star clusters—galaxies: interactions— galaxies: active—galaxies: starburst

1. Introduction

One of the most important results from the *Infrared Astronomical Satellite*[1] (*IRAS*) all-sky survey was the discovery of a significant population of galaxies that emit the bulk of their luminosity in the far-infrared (e.g. Soifer et al. 1984). Studies of the properties of these "infrared galaxies" showed systematic trends coupled to the total far-infrared luminosity; more luminous systems were more likely to appear to be merger remnants or interacting pairs, and were more likely to possess AGN-like emission line features. A more complete review of the properties of luminous infrared galaxies is given by Sanders & Mirabel (1996). Much attention has been focused on so-called ultraluminous infrared galaxies (ULIGs), objects with infrared luminosities, $L_{\rm ir}$,[2] greater than 10^{12} $L_\odot$, which corresponds to the bolometric luminosity of QSOs [3] (assuming the blue luminosity criterion $M_B < -22.1$, adjusting for our adopted cosmology: Schmidt & Green 1983). Multiwavelength observations of a complete sample of 10 ULIGs led Sanders et al. (1988a) to suggest that these objects might plausibly represent the initial dust- enshrouded stage in the evolution of optically selected QSOs, and that the majority, if not all, QSOs may begin their lives in such an intense infrared phase.

---

[1]The Infrared Astronomical Satellite was developed and operated by the US National Aeronautics and Space Administration (NASA), the Netherlands Agency for Aerospace Programs (NIVR), and the UK Science and Engineering Research Council (SERC).

[2]$L_{\rm ir} \equiv$ L(8–1000μm) is computed using the flux in all four *IRAS* bands according to the prescription given by Perault (1987); see also Sanders & Mirabel (1996). Throughout this paper we use H_o = 75 km s^{-1}Mpc^{-1}, q_o = 0.5 (unless otherwise noted).

[3]Based on the bolometric conversion $L_{\rm bol} = 16.5 \times \nu L_\nu$(B) of Sanders et al.(1989) for PG QSOs. Elvis et al. (1994) indicates a value of 11.8 for UVSX QSOs, increasing M_B to -22.5.

Considerable attention has been devoted to so-called "warm" systems, which have mid- infrared colors $f_{25}/f_{60} > 0.2$. [4] Sanders et al. (1988b) found that these systems predominantly have AGN optical spectra, very large molecular gas masses, ($M_{H_2} \sim 10^{10} M_{\odot}$), and advanced merger morphologies, and postulated that they represented the immediate transition phase between ULIGs and optically-selected QSOs.

An examination of deep far-infrared flux-limited samples such as the $f_{60} = 1$ Jy survey (Kim & Sanders 1998), however, shows that the majority (80% ; 90/115) of ULIGs are "cool" systems (i.e., $f_{25\mu m}/f_{60\mu m} < 0.2$). Thus, these galaxies are similar to the majority of ULIG systems previously studied by others (i.e. Sanders et al. 1988a, Kim 1995), rather than the smaller fraction of "warm" AGN-like systems like those discussed by Sanders et al. (1988b), Surace et al. (1998; hereafter Paper I) and Surace & Sanders (1999a; hereafter Paper II). Results derived in this paper for a sample of "cool" ULIGs are therefore likely to reflect the properties of ULIGs as a whole. In Paper II it was discussed that the warm ULIGs were possibly a transition state between cool ULIGs and QSOs. If this is true, then the cool ULIGs are expected to have properties similar to, yet less evolved than, the warm sample.

Many of the cool ULIGs have been imaged before at optical (Sanders et al. 1988, Kim 1995, Murphy et al. 1996) and near-infrared (Carico et al. 1990, Kim 1995, Murphy et al. 1996) wavelengths. However, these observations suffered from poor spatial resolution (FWHM $\geq 1.0''$) and lack of depth. Their wavelength coverage was limited predominantly to R and K-band, and was insufficient to disentangle reddening effects from intrinsic colors. Finally, several of the objects in the cool sample presented here have never been imaged before.

We present here new multiwavelength observations with 1.5 and 4× the spatial resolution of previous ground-based observations at optical and near-infrared wavelengths; despite being ground-based, they allow us to isolate interesting features such as the star-forming knots detected in the warm ULIG sample.

2. The Sample

A sample of 18 "cool" (i.e., $f_{25\mu m}/f_{60\mu m} < 0.2$) ULIGs was drawn from the *IRAS* Bright Galaxy Sample of Sanders et al. (1988) as well as the IRAS 1-Jy sample (Kim & Sanders

[4]The quantities f_{12}, f_{25}, f_{60}, and f_{100} represent the *IRAS* flux densities in Jy at 12 μm , 25 μm , 60 μm , and 100 μm respectively.

1998). The cool ULIG sample was chosen to complement the samples of "warm" ULIGs and infrared-excess PG QSOs as part of a study of the possible evolutionary connection between ULIGs and optically-selected QSOs (Surace 1998). A key observational fact known from spectroscopic studies of the larger parent samples is that cool ULIGs, warm ULIGs, and PG QSOs are known to represent a spectroscopic sequence that ranges from objects whose distribution of spectral types is biased towards H II-like spectra (HII-40%, LINER-40%, Sy2-20%; e.g. Veilleux, Kim, & Sanders 1999), to objects dominated by Seyferts (HII-10%, LINER-20%, Sy2-40%, sy1-30%; Veilleux et al. 1997), and finally to optically-selected Sy 1s (Schmidt & Green 1983; i.e. part of the definition of QSOs). The 18 cool ULIGs discussed here have a similar distribution of spectral types (HII-54%, LINER-35%, Sy2-11%)as their parent sample. The "warm" sample has been discussed previously in Papers I & II, and the infrared-excess PG QSOs are the subject of a forthcoming paper.

All of the "cool" ULIGs have been chosen to lie within the volume $z < 0.16$. This is the same volume limit as the "warm" ULIG sample of Paper I, and is very close to the completeness limit for ULIGs in deep *IRAS* surveys. Also, this is sufficiently nearby that the spatial resolution achievable from the ground can provide information on scales known from Papers I & II to be physically meaningful (typically a few hundred parsecs). Since there are over 100 such ULIGs known, this sample was selected first to include the original 7 cool ULIGs in the BGS sample, as these are most well-studied. The remaining cool ULIGs were selected such that their redshift distribution was similar to the "warm" ULIG and PG QSO samples of Sanders et al. (1988b) and Surace (1998). Specific objects were randomly chosen to lie in regions of the sky more amenable to observation from Mauna Kea, and to ameliorate crowding of the observing program in spring. Since this selection criterion is unrelated to the physical properties of the ULIGs, it should not bias the sample.

3. Observations and Data Reduction

The data were taken between October 1995 and March 1998 at the f/31 focus of the UH 2.2m telescope using a fast tip/tilt image stabilizer. This image stabilizer consists of a piezo-driven secondary with a pick-off mirror and guider ccd for guide-star acquisition. It is described by Jim (1995) and Pickles et al. (1994), and was used for the observations of Papers II & III. When used in off-axis guiding mode, it eliminates common-mode vibration of the telescope, as well as some seeing effects. This results in near-diffraction limited imaging (FWHM $\approx 0.3''$) in the near-infrared most of the time, since the seeing at the UH 2.2m site is extremely good. The system is not as effective at optical wavelengths, where the seeing is much poorer. The spatial resolution at I-band is typically 0.5-1$''$, with 0.75$''$

being typical. At B- band it is usually 1″.

The near-infrared data were taken with the QUIRC 1024×1024 HgCdTe camera in a manner identical to that of the "warm" ULIG sample in Paper II. The observations were made at H (1.6μm) and K′ (2.1μm). The H filter was chosen since it is the longest wavelength filter which is still relatively unaffected by thermal dust emission; dust hot enough to emit significantly at this wavelength would be above the dust sublimation temperature. The choice of the University of Hawaii K′ filter, which is bluer than both the Johnson K and the 2MASS K_S, was motivated by the lower thermal sky background in the K′-band (Wainscoat & Cowie 1992). This improves the detectability of faint features such as star-forming knots. Throughout this paper we exclusively refer to K′. Comparison to work by other authors is made using the conversion of Wainscoat & Cowie (1992).

The near-infrared data were reduced in the same manner as that described in Paper II. The data was initially sky-subtracted using consecutive, dithered frames; because the QUIRC field of view is so large (60″), it was possible to dither the target on- chip, thereby increasing telescope efficiency by a factor of 2. The images were then flattened using median flats constructed from images of the illuminated dome interior. Each image was masked by hand to exclude bad pixels and regions contaminated by negative emission introduced by the sky subtraction. The images were aligned using the IMALIGN task in IRAF, which uses a marginal centroiding routine that calculates a best fit solution to a number of (user-supplied) reference stars in the field. Typical alignment errors were estimated (on the basis of the fit) to be about 0.25 pixels. Given that the data was typically sampled by 5 pixels FWHM for a point source, alignment errors are unlikely to be important. Images were scaled according to their exposure times and then, in order to account for any variable sky background, an offset was subtracted from each image based on the background measured in that frame. The images were combined by medianing using IMCOMBINE and rejecting pixels outside the linear regime of the array.

The optical data were taken with several different instrument configurations. The UH Tektronix 2048 and Orbit 2048 cameras were used at the f/31 focus of the UH 2.2m. In both cases, the data were binned 2×2 in order to provide better spatial sampling (with adopted binned pixel sizes of 0.14″ and 0.09″, respectively). The Orbit 2048 was also used in conjunction with the HARIS spectrograph; by withdrawing the dispersion components it was possible to image through the spectrograph. The telescope f/31 beam was reimaged at f/10 resulting in an unbinned image scale of 0.14″ pixel^{-1}.

The optical data reduction involved several steps. First, the CCD bias pattern was removed by subtracting from each image a high S/N median bias frame constructed from sequences of 20-30 bias frames taken at the beginning and end of each night. Pixel-to-

pixel response variations were then corrected by dividing each image by a high S/N flat produced by making dithered observations of the twilight sky in each filter. Typical twilight exposures were 2-3 seconds each, short enough to avoid getting detectable flux from field stars, yet long enough to avoid flat-field errors introduced by the radial shutter used at the UH 2.2m. Estimated S/N for the flats (based on Poisson statistics and the gain of the CCD) was between 250-500. Neither CCD showed any evidence of measurable dark current, based on an examination of long closed shutter exposures. The images were then corrected to normal orientation by transposition and rotation using the ROTATE task in IRAF based on the known field rotation of the cassegrain focus of the UH 2.2m, which is accurate to better than 1 degree. The CCD overscan regions were trimmed using IMCOPY. The images were shifted and aligned using the method detailed above for the near-infrared data. The images were then averaged using an algorithm that rejects pixels inconsistent with the known noise properties of the CCD, allowing for rejection of cosmic rays. The shifted images were combined onto a larger image than the original data frames, thereby increasing the total field of view due to the dithering process. This was valuable primarily in order to increase the availability of PSF stars, since the size of the camera focal plane was much larger than the measurable extent of any of the galaxies.

In some cases the telescope cassegrain focus was rotated during the night in order to acquire brighter guide stars, thereby allowing faster guide rates and improving quality of the tip/tilt guiding. Additional flats were made, whenever feasible, at the rotation angles used. This was necessary since changes in the illumination of dust and other defects in the telescope optics tended to produce notable changes in the flat-field response, resulting in a strong background gradient in the vicinity of any optical defects such as dust.

The data were calibrated through observations of standard stars in the optical and near- infrared (Landolt 1983, 1992, Elias et al. 1982). Typically, 4–5 standard stars were observed throughout the night at airmasses similar to those of the science targets. The stars were interleaved with the science targets; such a strategy also enabled them to be used for refocussing the telescope. In most cases the nights were photometric with 1σ uncertainties in the photometric calibration of 0.05 magnitudes. For non- photometric nights, the data was calibrated by forcing agreement with large-aperture photometry already in the literature. In particular, the optical data for UGC 5101 were calibrated using Sanders et al. (1988a), while the IRAS 00091-0738 and IRAS 01199-2307 data were calibrated using the photometry of Kim (1995). K-corrections have not been applied to any magnitude reported in this paper. Since the most distant object is at redshift z=0.16, K-corrections are likely to be quite small. For a 10 Myr old starburst of the sort discussed below at the median redshift, the K-corrections are δ_M(B,I,H,K$'$)=(0.12,0.13,0.07,-0.11), and for a 2 Gyr old starburst population they are δ_M(B,I,H,K$'$)=(0.61,0.19,0.08,-0.16).

Kim (1995) and Trentham et al. (1999) computed K-corrections based on very large aperture spectra for ULIGs at redshifts similar to this sample, and found that optical K-corrections were typically less than 0.25 magnitudes, and near-IR K-corrections were less than 0.1 magnitudes. In order to make it easier to compare the measurements in this paper to those of others, magnitudes are presented without the uncertainty introduced by an assumed spectral shape. While the bandpass compression term is known for each ULIG, the inclusion of a bandpass compression-only, "pseudo K-correction" is omitted since the possible confusion it would create outweighs the very small advantage of including it.

The point-spread-function (PSF) was calibrated with actual stars in the final combined science image using DAOPHOT in the manner described in Paper II. All of the stars were identified, scaled, shifted, and combined using a sigma-clipping algorithm and weighting according to total flux, thus creating as high a S/N PSF image as possible. In those few cases where no stars were found in the science images, the PSF was estimated by using the closest temporally adjacent standard star. Since the tip/tilt guiding has little effect on atmospheric distortions at short wavelengths, this technique works well for optical data. Similarly, since the seeing remains stable on timescales of many minutes, this technique is also effective in the near-infrared.

Additionally, some of the cool ULIGs have been observed by *HST*/WFPC2 through the F814W (*I*-band) filter as part of the Borne et al. (1997) ULIG snapshot survey and are publicly available from the *HST* archive (see Table 1). These data were reduced in the same manner as the WFPC2 data in Paper I. These data were included primarily for comparison with the ground-based data. Since they are only at a single wavelength corresponding directly to one of our ground-based filters, they cannot be easily used for the multiwavelength color analysis presented here. Their spatial resolution is too high to allow a direct comparison without significant aperture effects.

In two cases we do not have complete data. Near-infrared data was not taken of Arp 220 because it had already been observed with *HST/NICMOS* (Scoville et al. 1998); this data has been retrieved for use here. Mrk 273 was not observed in the near-infrared because it had already been observed with adaptive optics from CFHT (Knapen et al. 1997).

As in Paper II, in some cases high spatial resolution techniques such as deconvolution were applied to the data in order to enhance detectability of features. The Richardson- Lucy algorithm implemented in IRAF/STSDAS was used along with the data-derived PSFs. It was allowed to iterate 20–50 times until noticeable artifacting appeared. Previous use of this technique has shown the observed structure to be reliable; in the case of the 6 systems with data from WFPC2 this was checked directly. Magnitudes and colors were not derived from the deconvolved data; rather, the deconvolved data was used to clarify morphological

details. The actual photometry was measured from the raw data using aperture photometry and PSF-derived aperture corrections. For further details, see Surace (1998).

4. Results

4.1. Morphology

4.1.1. Large-Scale Features

Images of each ULIG in the "cool" sample in each of the four observed filters are presented in Figure 1. Figure 2 presents near-truecolor images constructed from the optical data, as by Surace et al. (1998). The B & I-band images were linearly interpolated to provide the color information, and the resulting truecolor images should appear similar to the actual colors perceived by the eye. [5] Despite having higher spatial resolution, the near-infrared morphology is more featureless; therefore a near- infrared color image was not included.

The cool ULIGs exhibit a wide variety of morphologies, the details of which are tabulated in Table 2. At least 6 of the 14 systems (43%) have obvious double galaxy nuclei as evidenced by the manner in which tidal tails and spiral structure are centered on high surface brightness, extended emission regions. This is similar to the value of 47% found by Murphy et al. (1996) for a sample of 53 non far-infrared color-selected ULIGs. However, an additional 4 systems *may* have double nuclei, which would bring the total double nucleus fraction to as high as 72% (10/14).

Projected separations of the definite double nuclei span an order of magnitude from 25 kpc in IRAS 01199−2307 to just 2.5 kpc in IRAS 22491−1808. In all cases the double nucleus systems have extended tidal structure indicating that these systems have already passed initial perigalacticon and are now in an advanced merger state. None of the systems which appeared to have single nuclei from previous observations were found to have double nuclei when observed at higher spatial resolution. This may be an effect of confusion. As noted in Paper I and illustrated by the cautionary tale of Mrk 231 (Armus et al. 1994), it is difficult to differentiate true galactic nuclei (spheroidal bulge remnants) from unresolved

[5]Human vision is adapted to understand three-dimensional structure in terms of simultaneous luminosity and color information, and thus such true-color images provide the most intuitive means of understanding the structure of the star-forming regions and the reddening resulting from embedded dust (Kandel et al. 1991, Malin 1993).

aggregates of luminous, dusty young star-forming regions. Conversely, at the median redshift of the sample, typical spatial resolutions of 0.4″ at K′ are ≈ 600 pc, so at least a few systems with projected separations of 0.5-2 kpc should be expected. Even in the most confused of cool ULIGs (IRAS 22491−1808), the two galaxy nuclei can be clearly differentiated from the star-forming clusters on the basis of their K′ emission. Furthermore, the extremely high spatial resolution HST observations of three of the single nucleus objects also fail to detect additional nuclei. There are several apparently single nucleus systems which have extended optical nuclear regions with apparent bifurcating dust lanes which are very similar in appearance to the bifurcated core of IRAS 05189−2524. It is possible that the original progenitor galaxy nuclei lie in this chaotic central region if they have not already coalesced since they are not anywhere else in the system, and it seems unlikely that either heavy dust obscuration or a remarkable alignment along the line-of-sight could hide them. In the case of the nearest such system, Arp 220, the nuclei are actually known to be hidden in the optical structure.

The failure to discover any additional systems with previously unknown double nuclei when observed with the much higher spatial resolution of the near-infrared observations is similar to the result found in Paper I for warm ULIGs newly observed by *HST*. In order to evolve from the very widely separated systems to the single nucleus merger systems, the ULIGs must pass through a stage where the nuclei are separated by 0.5-2.5 kpc. If we assume an even distribution of physical separations between 25 kpc and fully merged systems, then the probability of selecting at random a sample with as few small-separation systems as observed here is much less than 1% (based on monte carlo simulations). This implies a bimodal distribution in separations for the underlying distribution of ULIGs. This may indicate that the timescale for final coalescence of the nuclei is comparatively short, and as a result there is a natural depletion in intermediate separation systems. Alternatively, the ULIG luminosity selection criterion may be selecting two different populations — systems that are ultraluminous at large separations, and systems that are ultraluminous only after merger.

None of the cool ULIGs shows evidence for the same kind of bright, extremely compact AGN-like nuclei as are found in several of the warm ULIGs such as Mrk 231. However, the *HST* images of Mrk 273 and UGC 5101 (Figure 3) reveal that both of these systems have single, very compact (radius ≈ 100 pc) high surface brightness features at *I*-band in their nuclear regions. Because there is also considerable structure in the nuclei of these systems, our ground-based *I*-band images with limited spatial resolution cannot spatially separate these central nuclei from their luminous surroundings. Similarly, both our ground-based images and the *HST* data show the presence of a nearly unresolved object in IRAS 12112+0305. IRAS 23365+3604 also appears to have very compact nuclear

structure, although it also has one of the lowest percentages of its total emission in its central 2.5 kpc region. These results point to the presence of compact "nuclei" in a small percentage (28%) of the cool ULIGs that are morphologically similar to the most extended, low surface brightness "nuclei" in the warm ULIGs, such as IRAS 12071−0444 and IRAS 15206+3342. Three of these four cool ULIGs are single nucleus systems (Mrk 273, UGC 5101, and IRAS 23365+3604), and all four have considerable numbers of star-forming knots visible near their nuclei in the *HST* data; all of these are suggestive of transition objects between the greater population of cool ULIGs (e.g., IRAS 14348−1447) and the AGN-like compact-nucleus warm ULIGs (e.g., Mrk 231). That two of these systems (Mrk 273 and UGC 5101) are the only two cool ULIGs with known Seyfert spectra makes this explanation even more compelling (Sanders et al. 1988a, Khachikian & Weedman 1974).

All 14 systems show well-developed tidal tails and plumes. Many of these tails are curved to form circular or semi-circular ring-like structures, and it is likely that many of the linear tails are similar structures seen edge-on. The tails have total projected lengths averaging 35 kpc and ranging from 9 kpc to 100 kpc; the ringlike structures are generally 15-30 kpc in radius. In almost every case, these tidal features appear to be circular rings or ring segments oriented nearly perpendicular to each other. In addition to these obvious cases where the disks and tails lie in a plane either parallel or orthogonal to the projected plane of the sky, many of the other galaxy systems can be explained as projections of this same geometry combined with additional rotation. In many cases it appears that the progenitor galaxies may have been rotating in opposite directions, judging from the opposing opening angles of the tidal tails, which have presumably inherited the angular momentum of their progenitors (e.g., IRAS 01199−2307, IRAS 23233+0946). Figure 4 shows an n-body simulation taken from Barnes (1992). The upper left panel shows the model disk encounter geometry, which may be similar to that of many of the cool ULIGs, while the bottom right panel shows the cool ULIG UGC 5101 at I-band for comparison.

4.1.2. Star-Forming Knots and Small-Scale Structure

Many of the systems show evidence of the same clustered star formation seen in the "warm" ULIGs. Only four show no obvious high surface brightness compact knot-like features. Since these are the four systems at the highest redshifts ($z > 0.13$), this may be an effect of the limited spatial resolution achievable from the ground; however, the physical spatial resolution for IRAS 00091−0738 is nearly as poor at $z = 0.12$, yet it shows considerable evidence for star-formation. Moreover, these systems are 4 of the 6 double nucleus systems and 3 of them have the largest projected separations, which may indicate a

lack of clustered star formation in mergers with large nuclear separations. This is similar to other results which indicate that there may be a delay in star formation until some time after the first contact between galaxies (Joseph et al. 1984, Surace & Sanders 1999b). The role of star formation as characterized by far-infrared activity in very widely separated pairs is discussed widely in the literature (Bushouse et al. 1988, Haynes & Herter 1988, Surace et al. 1993). Figure 5 illustrates Richardson-Lucy deconvolved data for these star-forming regions. Figure 3 presents images of the *HST*/WFPC2 data for our sample objects, which can then be compared to the ground-based images in Figure 5.

In order to be recognized as real features in the deconvolved images, the small-scale structure must at least be recognizable in the undeconvolved images. This provides a means of allowing the real features to be discriminated from the amplified, highly- correlated noise that produces the "mottling" effect in the deconvolved data. As in Paper I, the knots are defined as compact emission sources with closed isophotes that are more than 3σ above the local background in the undeconvolved images. This distinction is made in an attempt to discriminate between the "knots", which appear to be compact bursts of star-formation, and the more extended "condensations" which appear to be a result of large-scale tidal structure. Examples of condensations can be seen in the southern arc of IRAS 12112+0305 and the western tail of UGC 5101. As was noted in Paper I, it is likely that all of the "knots" are actually unresolved aggregates of star- forming clusters like those seen in other, more nearby interacting galaxies. Given the even poorer spatial resolution of the ground based images (as opposed to those from *HST*), many of the star-forming knots are likely to be even more confused than in Paper I and this limits our ability to recognize the star-forming knots. Because of this, the analyses of the luminosity functions, etc., as was carried out in Paper I, cannot be repeated here meaningfully. Table 4 gives aperture photometry for the star-forming knots that could actually be recognized as such; it probably misses many more. It also does not list photometry for features that appeared to be more extended tidal structure, although in many cases there appears to be tidal structure in the form of arms and wisps even at very small scales. Details of this additional structure are discussed in §4.2. Positions are given relative to the brightest feature in I-band and correspond to the apparent galaxy "nucleus".

Most of the star-forming knots are within a radius of a few kpc of the nuclei, a result suspected from previous aperture photometry studies which showed systematic color changes at small galactocentric radii (Carico et al. 1990). As in the warm ULIGs, knots and condensations are also seen along the tidal features; this is particularly apparent in IRAS 00091−0738, UGC 5101, Mrk 273, IRAS 12112+0305, IRAS 14348−1447, and IRAS 22491−1808.

4.2. Luminosities

The "cool" ULIGs do not show morphological evidence for the compact putative AGN found in the "warm" ULIGs. Instead, most of the "nuclei" appear to be extended with evidence of starburst activity, based on their colors as detailed below. Furthermore, many of the nuclei have complex morphological structures similar to star-forming regions. Therefore, only the luminosities of the host galaxies and the star-forming knots are discussed since a comparison between the nuclei and AGN is unwarranted.

4.2.1. Host Galaxies

Luminosities were computed using the formula given in Paper I (equation 1), which corrects for distance but does not include K-corrections. As in Paper II, we consider the H-band luminosity as the best indicator of the total mass of the old stellar population, and hence the combined mass of the merger progenitors. It additionally is much less affected by extinction than shorter wavelength observations, and K-corrections at H- band are likely to be less than 0.1 magnitude based both on a modeled starburst population and also on the empirical results of Kim (1995). Unfortunately, this is somewhat more complicated in the case of the cool ULIGs than it was for the warm ULIGs and will be for quasar host galaxies (e.g. Surace (1998), Surace & Sanders (1999a)) . In particular, since the warm ULIGs each appeared to contain a compact AGN-like nucleus, it was easy to subtract this nuclear component, as well as any emission from compact star-forming knots, from the extended host galaxy. In the case of many of the cool ULIGs, there is not a clear AGN component. Instead, the "nuclei" of the cool ULIGs often appear to be diffuse, extended regions with complex structure; a large fraction of the luminosity in the nuclear regions is likely to be old starlight, in which case it should not be subtracted from the global H-band luminosity.

Several approaches are considered in computing the total H-band luminosity of the host galaxies. First, the total flux at H-band, including any star-forming knots, galaxy nuclei, etc. is considered. This will set an upper limit on the host galaxy luminosity, since it must necessarily include additional young stellar population components. The integrated photometry was derived by measuring the total flux of the system in an aperture large enough to encompass the optical extent of the galaxy at a flux level below 1 σ. Errors in total luminosity are typically 0.07 magnitudes. These values are given in Table 3. In this way it is found that the cool ULIGs are similar in luminosity to the warm ULIGs. In Paper II the H-band luminosity of an L^* galaxy was estimated to be between $M_{\rm H}$=−23.8–24.1; we adopt here $M_{\rm H}$=−23.9. The cool ULIGs are found to have total luminosities ranging from $M_{\rm H}$=−23.38 (Arp 220) to $M_{\rm H}$=−24.70 (IRAS 14348−1447, IRAS 22206−2715), with a

mean value of $M_{\rm H}$=−24.23. This range is from 0.6–2.1 L^*, with a mean of 1.4 L^* and with roughly half of the ULIGs lying between 1.5–2.5 L^*. However, there are no 5–7 L^* systems as there were with the warm ULIGs.

This result is complicated by the finding that the colors of the nuclear regions of the cool ULIGs are consistent with a line-of-sight extinction of $A_{\rm V}$ = 2–5 magnitudes (see §4.3). As was indicated in Paper II for IRAS 08572+3915, it is therefore likely that the unreddened global values derived above are slight underestimates. One visual magnitude of reddening corresponds to $A_{\rm H}$ = 0.18 magnitudes (Reike & Lebofsky 1985). In the most extreme (hypothetical) case that all of the luminosity lay within the inner 2.5 kpc (since these reddening values were determined inside this region), then dereddening would at most increase the luminosity of the galaxies by 1 magnitude at *H*. In actuality this effect is much more modest, as can be demonstrated by dereddening just the observed luminosity in the nuclear regions and adding this to the outer galaxy luminosity; typically this increases the galaxy luminosity by 0.1 magnitudes, ranging from 0.08 in IRAS 23233+0946 to 0.4 in UGC 5101. The dereddened luminosities then range from $M_{\rm H}$=−23.8 to $M_{\rm H}$=−24.9 or 0.9–2.5 L^*. Excluding the anomalous case of IRAS 01003−2238, this is very similar to the range found for the warm ULIGs, and is consistent with the merger of two galaxies, a result also suggested by the extended morphologies of the ULIGs.

At the other extreme, it is possible to examine the luminosity of the outer galaxy by simply excluding all of the flux in the 2.5 kpc diameter nuclear region. On average, 37% of the H-band flux lies within a radius of 1.25 kpc of the center of each ULIG, varying from 52% (IRAS 00091−0738) to 17% (IRAS 23365+3604). Excluding the central regions, the luminosity of the outer regions of these galaxies range from $M_{\rm H}$=−23.0 (0.4 L^*) to $M_{\rm H}$=−24.5 (1.7 L*). Obviously, these are considerable underestimates — the previous dereddened results are probably closer to the truth. Furthermore, the fraction of H- band light inside the central regions is similar to that found in the bulges of disk galaxies (Kent 1985), further indicating that the central region contains a considerable amount of old starlight.

4.2.2. Star-Forming Knots

The star-forming knots have *B*-band luminosities ranging from $M_{\rm B}$=−14.4 to $M_{\rm B}$=−18.5, which is similar to or slightly higher than those observed for the "warm" ULIGs. The higher values are likely to result from confusion. The more limited spatial resolution of the ground-based optical observations (typically 0.7–0.8″at *B*) yields a physical resolution of 1 kpc at the median redshift. Any given knot optically detected from the

ground is therefore likely to contain at least several of the knots detected by *HST*. An examination of Figure 3 confirms that in some cases (i.e., Mrk 273) this occurs, while in others (IRAS 22491−1808) this effect may be much less. Also, in Paper I it was found that the luminosity function of the knots continued to increase until reaching the detection limit of $M_{\rm B}$=−12, but confusion and limited spatial resolution prevent our reaching such low detection limits. Finally, any differences in the ages of the stellar populations of the knots would be expected to change their luminosities by several magnitudes. The total integrated luminosity of the star-forming knots (the sum of all knot luminosities) at B-band ranges from $M_{\rm B}$=−17.2 in IRAS 00091−0738 to $M_{\rm B}$=−19.5 in IRAS 14348−1447, with a median value of $M_{\rm B}$=−18.3. This is approximately 6 times more luminous than the mean integrated *B*-band luminosity of the knots in the warm ULIGs. The total fraction of the galaxy *B*-band luminosity found in the star-forming knots ranges from 6% to 25%, with a median of 11%. By comparison, the warm ULIGs vary from less than 1% (PKS 1345+12) to nearly 40% (IRAS 15206+3342), but this much larger spread in the total percentage is due to the presence of the putative active nuclei. The highest percentage (and total luminosity) are found in the two double nuclei with detectable star-forming knots: IRAS 22491−1808 and IRAS 14348−1447. This may be indicative of the increased luminosity of the knots with younger ages, if the presence of double nuclei actually implies younger age.

Very few of the knots are detected at near-infrared wavelengths. Significant numbers of detections occur only in IRAS 12112+0305, IRAS 15250+3609, and IRAS 22491−1808. The K-band luminosities for the detected knots range from $M_{\rm K'}$=−18.0 to $M_{\rm K'}$=−23.0, which again is similar to those found in most of the "warm" ULIGs. The implications of the non- detections are discussed below. The total integrated luminosity of the star-forming knots detected at K′ ranges from $M_{\rm K'}$=−18.0 to $M_{\rm K'}$=−23.5. Considering the upper limits imposed by the non-detections, the typical cool ULIG has an $M_{\rm K'}$ originating in the star-forming knots of no more than −21.2. In those warm ULIGs with knots detectable in the near-infrared, this same number varied from −20.6 to −24.0, a very similar range.

4.3. Colors

4.3.1. Models

A multi-color approach as used by Surace & Sanders (1999) is adopted here. The three colors (*B*−*I*),(*I*−*H*),(*H*−*K*′) define a spectral shape. Two representations of this color space are presented in Figures 6 & 7. These 3-color diagrams are the set of all possible SEDs that can be defined (within the upper and lower bounds of the axes) by the four photometric measurements. The tracks made by the models (described below) represent the subset of

all possible SEDs consistent with those models. Thus, the points on the model tracks lying closest to the real data represent the best possible fit of the data to the model. The two figures are identical and represent different rotations of the color space with respect to the line-of-sight-reddening vector. Figure 6 is rotated such that the plane of the page is orthogonal to this vector, and hence the location of a point in the projection of the 3-color space onto the page is independent of line-of-sight extinction. It is therefore possible to fit the data to the models independent of extinction. Figure 7 is rotated such that the vector lies in the plane of the page and thus allows an immediate estimate of the magnitude of line-of-sight extinction. The value of the two rotated projections is that they reduce the 3-color diagram to the more familiar 2-color diagram, only with the special property that they have separated the effects of line-of-sight extinction.

Figures 6 & 7 also show the colors of several modeled populations, as well as various reddening effects (see the figure caption). A more thorough explanation of these models is given by Surace & Sanders (1999). For comparison, the median colors of the "warm" ULIGs, which for reasons presented in Paper II are likely to be AGN viewed along a complex, lightly extinguished path, are shown with a large circle.

Rather than K-correct the data with an unknown SED, a different approach was used wherein the models were corrected instead. Since the models of the emission processes, starbursts, and QSOs have detailed SEDs, inverse K-corrections can be made to their rest-frame colors at the redshift of our targets. This is done by convolving the synthetic spectra with the known detector and filter bandpasses. The magnitude zeropoint calibration of the filters is derived using the Kurucz model spectrum of Vega (BC95). For brevity, Figures 6 and 7 are calibrated to the median ULIG redshift, z=0.1. The K-corrections affect the modeled stellar colors by $\delta(B{-}I,I{-}H,H{-}K')=(-0.01,0.06,0.18)$ for a young (10 Myr) starburst, and by (0.42,0.11,0.24) for an old (2 Gyr) population. The effects of K-corrections can therefore be quite large depending on the modeled population, and hence the representation of stellar colors made in Figures 6 & 7 can be considered to have a sizable uncertainty attached. Larger redshift values also shift the dust emission curves to a more vertical orientation, as the rest frame filter bandpasses become bluer. Actual comparisons to the models made in the text were performed using models corrected to the appropriate redshift.

4.3.2. Data

The same confusion over the definition of "nuclei" that plagues the determination of the underlying galaxy luminosity also creates problems for the color analysis. In order to

help eliminate redshift-dependence, "nuclear" is defined to mean the central region of the galaxy 2.5 kpc in diameter. At the redshift of the most distant object in our sample (z= 0.152), this corresponds to 0.8″, which under the worst conditions is roughly the size of one resolution element at optical wavelengths. The nuclear magnitudes were measured using circular aperture photometry, to which the aperture corrections derived from the PSFs were applied. The latter are the dominant source of error, and the nuclear magnitudes have uncertainties of 0.1 magnitudes. Table 3 also gives "nuclear" magnitudes in each of the 4 observed filters. The ($B-I$),($I-H$),($H-K'$) colors of the central 2.5 kpc regions of the cool ULIGs are shown in Figures 6 and 7.

Most of the cool ULIG nuclei have colors consistent with a young (10-100 Myr) stellar population combined with hot (800K) dust emission that contributes 30–40% of the K′ flux, or of a mixture of stars and absorbing dust with a total optical depth approaching $A_{\rm V}$ = 30–50 magnitudes. However, the more complete mixed stars and dust model with scattering that was discussed in Paper II indicates that it is difficult to achieve such reddened colors in this way, which strongly suggests that the ($H-K'$) excess is actually due to hot dust emission. These colors are similar to the range observed by Carico et al. (1990b) in the "LIGs" ($L_{\rm IR} > 10^{11}\ L_{\odot}$). Regardless of whether they are stars with additional hot dust emission or just stars mixed with extinguishing dust, they additionally appear to be reddened by a uniform foreground dust screen of A_V = 1– 5 magnitudes, which is considerably higher than any foreground screen found in the "warm" ULIGs for either the nuclei or the star-forming knots. The presence of a greater foreground reddening screen than that in the warm ULIGs is qualitatively consistent with the evolution scenario in which an obscuring dust screen is blown away from the initial merger state. Alone among the cool ULIGs, IRAS 22491−1808e appears to have optical/near- infrared colors almost identical to that of the median "warm" ULIG colors. This is possible evidence that IRAS 22491−1808 harbors an AGN, although its K′ luminosity ($M_{\rm K'} = -22.37$) is more than an order of magnitude fainter than that of a QSO (Surace 1998). It is perhaps surprising that UGC 5101 does not also have AGN-like colors. However, the *HST* images reveal structure in the vicinity of the compact *I*-band nucleus that cannot be resolved from the ground optically, and it is likely that this structure is contaminating our results. Results from NICMOS indicate that the point-like nucleus actually does have QSO-like colors (Scoville et al. 1999).

The colors of the star-forming knots are more problematic to analyze. This is because they are not as well determined as the nuclear colors due to their irregular shapes and small sizes, and because they are not detected in many cases in the near-infrared despite the superior resolution at long wavelengths. For the non-detections, the upper limits of the near-infrared luminosities of the knots constrain their colors, and hence their ages.

Figure 8 shows the ($B-I$),($I-H$) colors of the BC95 instantaneous starburst used in Papers I & II. It is apparent that for starburst colors of ($I-H$) < 1 the modeled starburst age is constrained to less than 10 Myrs. As noted in Paper I, with detections only at B and I and upper limits in the near-infrared, it is only possible to set upper limits to the knot ages; dereddening will always *decrease* the estimated ages. Many of the cool ULIGs with detectable star-forming knots (IRAS 00091−0738, UGC 5101, IRAS 14348−1447, IRAS 20414−1651, IRAS 22491−1808 and IRAS 23365+3604) have at least several knots whose ages cannot be more than 5–7 Myrs. However, several also have knots that are sufficiently red that their age limits can only be estimated to be less than 1 Gyr (UGC 5101, IRAS 12112+0305, Mrk 273, IRAS 22491−1808) or a few hundred Myrs (IRAS 15250+3609 and IRAS 22491−1808). Thus, while we can show the presence of young stars, we cannot easily determine a lower age limit and thus demonstrate the presence of intermediate age stars. Thepresence of young stars seems to be much more prevalent among cool ULIGs than among warm ULIGs. While this could arguably be an effect of greater reddening in the warm ULIGs, the results presented here run counter to this in that the cool ULIG nuclei seem to suffer greater foreground reddening than that found in the warm ULIGs.

5. Relationship of Optical/Near-Infrared Emission to Bolometric Luminosity

Surace & Sanders (1999) found that in many cases the putative AGN in the warm ULIGs could be made to account for the high bolometric luminosities of the systems by assuming a QSO-like SED and extrapolating from the observed optical/near-infrared luminosities. It is possible to apply similar techniques to the emission in the cool ULIGs. Starburst models are chosen since the optical/near-infrared colors appear to be characteristic of young stars. The bolometric luminosity will then be determined based on both empirical and theoretical models.

The theoretical SEDs are based on the BC95 models. As before, a modeled instantaneous starburst with a Salpeter IMF and upper and lower mass cutoffs of 0.1 and 125 $M_{\odot}$was used. For any given age, a bolometric correction (BC) can be determined from the models to derive a bolometric luminosity based on the luminosity in some specific filter. Figure 9 shows the bolometric correction as a function of age for K-band. It is immediately apparent that the bolometric correction (BC) hinges critically on the age of the starburst. Prior to 5 Myrs, the luminosity is dominated by short-wavelength emission from high mass OB stars; very little of the bolometric luminosity originates in the late-type stars that emit strongly at long wavelengths. At 10 Myrs this changes radically as the most massive stars age and emit the bulk of their luminosity at progressively longer wavelengths, and hence

the bolometric correction spans fully 6 magnitudes depending on the age. With this model, an ultraluminous starburst could have $M_K < -21.2$ for a young burst, or $M_K < -27$ for an old one. Ironically, the change in bolometric correction with age is much less at shorter wavelengths (Figure 9 also shows the BC as a function of age for B-band), but the uncertainty in luminosity caused by dust extinction at short wavelengths may offset any gain. It can be argued that ages of 10 Myrs and shorter for *all* of the knots are unlikely for several reasons. The cool ULIGs span a considerable range in interaction morphology. The presence of star-forming knots in most of these systems (as well as the more dynamically evolved, based on presence of single nuclei, warm ULIGs presented in Paper I), however, indicates that the star formation history for the knots as a whole must be similar to the dynamical timescale, i.e., hundreds of Myrs. Similarly, the wide range in colors seen in many of the knots in the ULIGs may be evidence for a spread in knot ages, although this may also be due to reddening.

While B-band observations are strongly affected by dust extinction (as noted earlier), we can constrain the maximum amount of foreground extinction on the basis that the starlight can only be dereddened to the colors of the bluest young starbursts. Most of the star-forming knots, therefore, cannot be dereddened by more than 2 magnitudes. This yields a fraction of the bolometric luminosity contributed by star-formation actually detected at B-band with a young (less than 10 Myr), dereddened starburst between 1% (IRAS 00091−0738) and 100% (IRAS 22491−1808), with a median value of 6%. If the starburst is older (100 Myrs), then these percentages fall by a factor of 6. An additional uncertainty results from the large geometric corrections to the luminosity discussed in Paper II. However, the scattering models indicate that it is relatively difficult to achieve the red colors observed in Figures 6 & 7 via a stellar ensemble mixed with dust alone, and that they are more likely to be a result of hot dust emission and foreground extinction. If the stars are embedded in a thick dusty medium then their luminosities are underestimated by factors of 3–6.

Results for the K-band are least affected by uncertainties in dust extinction, and hence should give the best luminosity estimate. We have examined those cases where star formation can be morphologically separated from the underlying host galaxy stellar population, i.e. those systems that show evidence for star-forming knots. The total K- band flux was dereddened by the amount indicated by the nuclear optical/near-infrared colors and then the portion attributable to starlight (typically 50–70%, again determined by the colors) was separated out. These extinction estimates are likely to be overestimates, given the high extinctions derived from the nuclear colors and the maximum extinctions derived from just the knot optical colors. As discussed above, the BC95 models cannot readily constrain the bolometric luminosity based on the K-band luminosity due to the enormous

age dependence of the BC. If the star-forming knots are very young, (less than 1 Myr), then every cool ULIG with detectable knots at K′ could conceivably derive its entire bolometric luminosity from the star-forming knots alone. The upper limits for the knots not detected at K′ can only constrain the bolometric luminosity under this assumption of extremely young stellar age to being just under the measured ULIG bolometric luminosities. If the knots are more than 10 Myrs in age, then it is likely that none of the ULIGs could have contributions to their bolometric luminosities by star-forming knots much above 50%, and in most cases it would be less than 10%.

The empirical model is based on the bolometric correction from K-band to $L_{\rm ir}$ found in the LIGs (Carico et al. 1990; equation 7 Paper II):

$$\log L_{\rm ir} = -\frac{M_{\rm K'} - 6.45}{2.63} \tag{1}$$

Assuming that nearly all (≈95%)of the bolometric luminosity is emitted in the far-infrared (Sanders et al. 1988a), this is equivalent to a bolometric correction of 0-0.3 for $M_{K'}$=−20 to −25, or roughly equivalent to the modeled value for a starburst 10 Myrs old (i.e. a BC of 0–0.3 will convert between $M_{K'}$ to $M_{\rm bol}$ in LIGs). Using equation 1, the derived total bolometric luminosity for the detected star-forming knots ranges from 10^{10} $L_\odot$ to $10^{11.4}$ $L_\odot$. The typical ULIG which has star-forming knots detected in *any* band has a contribution to the bolometric luminosity of not more than $10^{10.5}$ $L_\odot$. This falls short of the average cool ULIG bolometric luminosity by a factor of 50. It thus appears that *nothing* detected optically or in the near- infrared in the cool ULIGs is capable of generating the high bolometric luminosity assuming the kinds of SEDs we have used here. Note that this result does not preclude the existence of an ultraluminous starburst or AGN, since ultimately something must provide the known bolometric luminosity. Rather, this result implies that no such object is directly observable in the optical or near-infrared. Whatever the power source, it must be more highly obscured in the cool ULIGs than in the warm, a result supported by the estimated extinctions derived from the optical/near-infrared colors.

6. Conclusions

We have presented high spatial resolution images of a sample of "cool" ULIGs. We find that:

1. All of the systems are major mergers, as manifested by prominent tails and other extended tidal structure.

2. A large fraction (at least 43% and as high as 72%) have resolvable double galactic nuclei. Their projected separations span the range 2.5–25 kpc. Double nuclei could have been detected with separations as small as 600 pc. The lack of small- separation (0.6–2.5 kpc) systems may support earlier similar findings that indicate that the time for final coalescence of the nuclei is comparatively brief.

3. Most of the "cool" ULIGs have evidence for compact star-forming knots, with the exception of the systems with the widest separations. This may indicate that clustered formation begins in earnest only near the end stages of the merger, just before nuclear coalescence, although this result may also partly be due to the limited ground- based resolution.

4. The nuclear colors of most of the cool ULIGs appear similar to that of a mixture of stars and extinguishing dust with a total optical depth of $A_{\rm V}$ = 30–50 magnitudes, or of young stars with a modest amount of the K' emission (30%) originating in hot (800 K) dust. This hot dust emission is then further extinguished by a uniform dust screen $A_{\rm V}$ = 1–5 magnitudes thick. Unlike the "warm" ULIGs, the optical/near-infrared emission from the nuclear regions of the cool sample is probably stellar in nature.

5. The dereddened *H*-band luminosities of the cool ULIG host galaxies lie in the range 0.9–2.5 L^*, and are thus essentially identical to those of the warm ULIGs and are consistent with their apparent merger origin. There are, however, no systems with $L_{\rm H} > 3\ L^*$, unlike 25% of the warm ULIGs.

6. Very few of the star-forming knots are detected in the near-infrared, nor are any new knots (much like the "warm" ULIGs). Constraints imposed by the limits of their (*I*-*H*) colors imply very young ages (< 5–7 Myrs) for many of these knots. They cannot be extinguished by more than a very mild foreground reddening screen ($< A_{\rm V} = 2$ magnitudes), and any additional knots must be very deeply embedded.

7. As in the "warm" ULIGs, it appears that in most cases the star-forming knots are insufficiently luminous to be the source of the high bolometric luminosity, although in some cases they may provide a significant fraction. Although the constraints are found to be very model dependent, using assumptions similar to those used in Paper II, the observed optical/near-infrared emission observable in the knots provides typically only about 2% of the high bolometric luminosity, ranging from less than 1% to about 20%. This is very similar to the results found for the warm ULIGs. It appears unlikely that anything seen in the optical or near-infrared is related to the high bolometric luminosity, unless it has an SED much more biased towards the far-infrared.

We thank the creators of the tip/tilt system and the instruments, Kevin Jim and Gerry Luppino. We thank John Dvorak, Chris Stewart, and Rob Whitely for operating the telescope, and Andrew Pickles for helping debug numerous telescope-related problems. We thank Josh Barnes for his useful comments on early drafts of this text and Atiya Hakeem for proofreading it. We also thank Catherine Ishida and Alan Stockton for helping to supply observing time to complete these observations. We thank an anonymous referee whose comments helped improve the presentation of this paper. D.B.S was supported in part by JPL contract no. 961566 and J.A.S. was supported in part by NASA grant NAG5-3370.

A. Notes on Individual Objects

IRAS 00091−0738 — a system very similar in appearance to IRAS 12112+0305 with an extremely complex nuclear core 3.5 kpc in diameter bifurcated N-S by dust lanes. A thick, perhaps edge-on tail extends 19 kpc (projected distance) to the south, while another plume-like tail extends 20 kpc to the north. At near-infrared wavelengths the core becomes a single source 0.7″ in diameter, with a tidal tail to the north. This connects to and appears to be the base of the optical tidal tail which loops around back towards the south, and appears similar to the structure seen in the core of IRAS 12112+0305. Identified as having HII spectra by Veilleux et al. (1998).

IRAS 01199−2307 — double nucleus system separated by 25 kpc, the largest separation of any ULIG in this sample. Both nuclei are ellipsoidal in appearance and remain similar to spiral bulges; Veilleux et al. (1998) identifies these as having HII spectra. The NE nucleus is surprisingly faint in the near-infrared compared to the SW; additionally, at K′ it takes on the appearance of two lobes, the SW of which seems to correspond to the optical nucleus, and the NE to the arm extending from it. The western tail is 48 kpc in total length, with an apparent projected linear length of 40 kpc. The fainter eastern tail is 30 kpc long.

IRAS 03521+0028 — double nucleus system separated by 4.3 kpc. Short, stubby tails extend 9 kpc from each nucleus in an E-W direction. No additional star- forming knots or other structure are seen. This galaxy has LINER optical spectra (Veilleux et al. 1997).

UGC 5101 - a nearby system from the BGS, identified as a Seyfert 1.5 by Sanders et al. (1988a). A linear tail stretches 38 kpc to the west from the nucleus. A second tail runs clockwise from a position angle of -90 to form a nearly complete circle 225 degrees around with a radius of 17 kpc and a total length of 65 kpc. The optical morphology seems to suggest that the two sets of tails are actually similar features lying in planes perpendicular to each other. The *HST* images clearly reveal a set of spiral dust lanes to the north of the

nucleus; the nucleus itself is dominated by a small (200 pc) size emission region. This spiral structure, along with that in the core of Mrk 273, may resemble that seen in the warm ULIG Mrk 231 (Paper I), only rotated out of the plane of the sky.

IRAS 12112+0305 — this galaxy appears to consist of a double-lobed core similar to that seen in IRAS 00091-0738, with a bright tidal tail extending 18 kpc to the north and another arc 30 kpc long loops along the south. The orientation of the tails suggests that the northern tail is parallel to the line of sight, while the southern lies tilted by 45 °. The southern arc has a blue condensation halfway along its length. A red star-like object is located 4 kpc SW of the core. Seen by Carico et al. (1990), this is unlikely to be a supernova since it has not faded noticeably in the intervening 7 years. It is not a foreground star as recent near-infrared spectroscopy (Surace, in prep) indicates that it is at the same redshift as the nucleus to its north — if it is a starburst knot or AGN then its total lack of U′ emission indicates a line of sight extinction of at least $A_{\rm v} = 3$ magnitudes (Surace & Sanders 1999b, in press). Kim (1995) identifies this ULIG as having a LINER spectrum.

Mrk 273 — a very narrow ($\approx$ 2.5kpc) linear tidal tail extends 41 kpc south of the nucleus. Two diffuse plumes extend north and northeast 40 kpc each. The new deep images suggest that these plumes actually connect to the NE, making a complete ring nearly 100 kpc in circumference. In this respect it may be very similar to UGC 5101, which it strongly resembles. The *HST* image of the galaxy core at I- band clearly shows a pattern of dust lanes running along the long axis of the nucleus, closely resembling those seen in edge-on spiral galaxies. The nucleus is dominated by a small, yet extended emission region. Khachikian & Weedman (1974) identify this as a Seyfert 2. Several authors have shown evidence for an apparent double nucleus in Mrk 273 (Majewski et al. 1993 Condon et al. 1991), but more recent adaptive optics imaging at K-band indicates that this "nucleus" is more likely to be a luminous star- forming region (Knapen et al. 1997).

IRAS 14348−1447 — two nuclei separated by 5.3 kpc. A plume extends north 20 kpc from the NE nucleus. A second plume stretches 17 kpc to the SW from the SW nucleus, where it merges with a fan-shaped plateau of emission extending from the NE to the SW of the galaxy. At least a dozen star-forming knots are seen in the *HST* image. The circular ring of knots surrounding the SW nucleus are well detected in our B & I images, as are the knots in the base of the northern tail. We fail to detect these (or any other) knots in either near-infrared filter. Although Nakajima et al. (1991) claimed detection of a broad-line component in the SW nucleus, Veilleux et al. (1997) fail to confirm this and designate this galaxy as a LINER.

IRAS 15250+3609 — an apparently single nucleus system, this galaxy has at least three other galaxies nearby to the north, south and west. However, it is unclear if these

galaxies are physically related to the merger system. A tidal feature appears to emerge from the SW side of the nucleus and loops around on the eastern side to create a closed ring 27 kpc in diameter and 80 kpc long. Another, apparently shorter arm extends from the northeast of the nucleus. Near-infrared imaging reveals several additional knots of star formation near the nucleus. Veilleux et al. (1995) classify this as a LINER.

Arp 220 — the closest and hence most well-studied of all ULIGs. A short tail extends approximately 30 kpc to the northwest (Sanders et al. 1988a; Hibbard 1995). Graham et al. (1990) have shown evidence for a double "nucleus" in Arp 220. Recent NICMOS imaging of the same galaxy has shown two nuclei separated by 360 pc, along with considerable star formation (Scoville et al. 1998). Because this ULIG appears be radically different from most others in terms of its high degree of variable dust obscuration, the registration between our ground-based optical data and the NICMOS data is highly uncertain. Therefore, the 2.5 kpc aperture photometry should be regarded with caution; we have assumed that the bright near-infrared peaks are spatially coincident with the optical dust lane. Kim (1995) classifies this as a LINER galaxy. The reader is directed towards a wealth of literature on this object (Sanders et al. 1988a; Graham et al. 1990; Skinner et al. 1997; Scoville et al. 1998).

IRAS 20414−1651 — this complex system is somewhat different from the other ULIGs. It has a horseshoe-shaped main body with some sort of extended structure "corkscrewing" 17 kpc to the south, which then bends west and meets with a very blue stellar condensation. These condensations may be superimposed background objects, or newly formed high density regions in the tails themselves. Kim (1995) identifies this as having HII spectra.

IRAS 22206−2715 — two nuclei separated by 9.2 kpc. The northern nucleus is circular in shape, perhaps suggesting that it is viewed face on. The southern nucleus is elongated and bar-shaped, suggesting a spiral galaxy inclined by roughly 60°, an idea supported by the zig-zag nature of the tidal tail emanating from it. Each tail is approximately 20 kpc in total length. Like many of the other galaxies here, this seems to be a collision between two galaxies with high relative inclination, resulting in one broad, almost circular tidal tail, and one that is seen edge-on, or nearly so. Veilleux et al. (1998) finds this galaxy to have an HII spectrum.

IRAS 22491−1808 — the most extreme example of clustered star- formation in the sample. At optical wavelengths the knots of star-formation create so much confusion as to preclude identification of the galaxy nuclei. Only in the near- infrared do the two nuclei, separated by 2.5 kpc, stand out. The system has two high surface brightness tails. The first extends 12.5 kpc NE from the main body of the galaxy and is essentially featureless. The second extends NW 16 kpc from the main body, but ends in a complex, face-on circular

loop 10 kpc in diameter. This tail has two very red clumps of star formation at its base, and the circular disk at the end of the tail has many blue knots of star formation. The *HST* data seem to suggest that the NE tail may also terminate in a somewhat fainter version of this disk. This galaxy has an HII spectrum (Sanders et al. 1988a; Veilleux et al. 1995).

IRAS 23233+0946 — two nuclei separated by 8.5 kpc. A tidal tail 19 kpc in linear distance and apparently 28 kpc in total length extends to the SE. Both nuclei have colors consistent with an old stellar population. Veilleux et al. (1998) classify this as a LINER.

IRAS 23365+3604 — this galaxy has a single, point-like nucleus embedded in a face-on disk 20 kpc in diameter. Four large star-forming knots are contained in this disk, and are detected even in the near-infrared. The disk itself has a twisting spiral structure. A faint linear tail extends north for 60 kpc from the nucleus. Another, higher surface brightness tail extends 20 kpc due south from the nucleus. This tail has an odd projection halfway along its length — a short (few kpc) tail jutting west from its side, not unlike the feature seen in the linear tail of Mrk 273. Veilleux et al. (1995) classify this as a LINER.

REFERENCES

Barnes, J.E. 1992, ApJ, 393, 484

Barnes, J.E., & Hernquist, L. 1996, ApJ, 471, 115

Borne, K.D., Bushouse, H., Colina, L. & Lucas, R.A. 1997, BAAS, 191, 2102

Bruzual, G., & Charlot, S. 1993, ApJ, 405, 538

Bushouse, H.A., Lamb, & Werner, M.W. 1988. ApJ, 335, 74

Carico, D.P., Graham, J.R., Matthews, K., Wilson, T.D., Soifer, B.T., Neugebauer, G. & Sanders, D.B. 1990a, ApJ, 349, L39

Carico,D.P., Sanders, D.B., Soifer, B.T., Matthews, K., & Neugebauer, G. 1990b, AJ, 100, 70

Condon, J.J., Huang, Z-P., Yin, Q.F., & Thuan, T.X. 1991, ApJ, 378, 65

de Grijp, M.H., Miley, G.K., Lub, J., & de Jong, T., 1985, Nature, 314, 240

Elias, J.H., Frogel, J.A., Matthews, K. & Neugebauer, G. 1982, AJ, 87, 1029

Graham, J.R., Carico, D.P., Matthews, K., Neugebauer, G., Soifer, B.T., & Wilson, T.D. 1990, ApJ, 354, L5

Haynes, M.P. & Herter, T.1988, AJ, 96, 504

Hibbard, J.E. 1995, PhD. Thesis, Columbia, New York

Jim, K.T. 1995, BAAS, 187, 1394

Joseph, R.D., Meikle, W., Robertson, N.A., & Wright, G.S. 1984, MNRAS, 209, 111

Kandel, E.R., Schwartz, H., & Jessell, T.M., eds. 1991, Principles of Neural Science, (Elsevier: New York), 467

Kent, S.M. 1985, ApJS, 59, 115

Kim, D-C., 1995, PhD. Thesis, University of Hawaii

Kim, D-C., & Sanders, D.B., 1998, ApJS, 119, 41

Kim, D-C., Veilleux, S., & Sanders, D.B., 1998, ApJ, 508, 627

Khachikian, E.Y., & Weedman, D.W., 1974, ApJ, 192, 581

Knapen, J.H., Laine, S., Yates, J.A., Robinson, A., Richards, A., Doyon, R., & Nadeua, D. 1997, ApJ, 490, L29

Landolt, A. 1982, AJ, 88, 439

Landolt, A. 1992, AJ, 104, 340

Malin, D. 1993, Scientific American, 269, 72

Majewski, S.R., Hereld, M., Koo, D.C., Illingworth, G.D., & Heckman, T.M., 1993, ApJ, 402, 125

Murphy, T., Armus, L., Matthews, K., Soifer, B.T., Mazzarella, J.M., Shupe, D.L., Strauss, M.A., & Neugebauer, G. 1996, AJ, 111, 1025

Nakajima, T., Kawara, K., Nishida, M., & Gregory, B., 1991, ApJ, 373, 452

Pickles, A.J., Young, T.T., Nakamura, W., Cowie, L.L., et al. 1994, Proceedings of the SPIE, 2199, 504

Reike, G.H. & Lebofsky, M.J. 1985, ApJ, 288, 619

Sanders, D.B., Soifer, B.T., Elias, J.H., Madore, B.F., Matthews, K., Neugebauer, G., & Scoville, N.Z. 1988a, ApJ, 325, 74

Sanders, D.B., Soifer, B.T., Elias, J.H., Neugebauer, G.,& Matthews, K. 1988b, ApJ, 328, 35

Scoville, N.Z., Evans, A.S., Dinshaw, N., Thompson., R., et al. 1998, ApJ, 492, L107

Scoville, N.Z., Evans, A.S., Thompson, R., Rieke, M., Hines, D., Low, F.J., Dinshaw, N., & Surace, J.A. 1999, AJ, in press.

Skinner, C.J., Smith, H.A., Sturm, E., Barlow, M.J. et al. Nature, 386, 472

Surace, J.A. 1998, Ph.D. Thesis, University of Hawaii

Surace, J.A., Mazzarella, J.M, Soifer, B.T., & Wehrle, A.E. 1993, AJ, 105, 864

Surace, J.A., Sanders, D.B., Vacca, W.D., Veilleux, S., & Mazzarella, J.M., 1998, ApJ, 492, 116 (Paper I)

Surace, J.A., & Sanders, D.B., 1999a,ApJ, 512, 162 (Paper II)

Surace, J.A., & Sanders, D.B., 1999b, AJ, in press (Paper III)

Toomre, A., 1978, in "IAU Symposium: The Large Scale Structure of the Universe", (D. Reidel Publishing Co.: Dordrecht), 79, 109

Veilleux, S., Kim, D-C., & Sanders, D.B, Mazzarella, J.M., & Soifer, B.T., 1995, ApJ, 98, 171

Veilleux, S., Kim, D-C., & Sanders, D.B., 1998, ApJ, in press

Veilleux, S., Sanders, D.B., & Kim, D-C. 1997, ApJ, 484, 92

Fig. 1.— Optical (B,I) and near-infrared (H,K′) images of the "cool" ULIGs showing their large-scale structure. Northeast is at top left. All of the images for a given object except for Arp 220 and UGC 5101 are at the same scale, with ticks 2″ apart and major ticks every 10″. The physical scale bar on each of the B-band images is 10 kpc in length. Contours are logarithmic and illustrate the high surface brightness morphology.

Fig. 2.— Near-truecolor images of the "cool" ULIGs constructed from the B & I- band data. The galaxy SEDs have been linearly interpolated from the B and I data; the color balance is not absolute.

Fig. 3.— *HST*/WFPC2 archival F814W (I-band) images of ULIGs from the "cool" ULIG sample. Each tick mark is 1″, and the physical scale-bar is 2.5 kpc. Orientation is with northeast at upper-left.

Fig. 4.— An illustration of the possible ULIG merger progenitor geometry: a plunging collision between two disks highly inclined to each other. At upper left is a schematic representation of such a collision. Two disks are inclined at nearly right angles to each other and meet in a slightly off-center (non-zero impact parameter) plunging encounter. Upper right and bottom left show two orientations of the same 1.4 Gyr-old collision between two spiral galaxies, one of whose disks is in the orbital plane, and the other inclined to it by 71 °(Barnes 1992, Barnes & Hernquist 1996). This type of encounter raises a nearly circular, off-center tail structure in the lower left galaxy as a result of the plunging orbit (Toomre 1978). At bottom right is an I-band image of UGC 5101 for comparison.

Fig. 5.— Selected images of high spatial resolution structure in the nuclear regions of the cool ULIGs. All of the optical data except IRAS 12112+0305 and Mrk 273 has been deconvolved with the Richardson-Lucy maximum likelihood algorithm. The physical scale-bar is 2.5 kpc in length. Tick marks are every 2″ with major ticks every 10″.

Fig. 6.— ($B-I$,$I-H$,$H-K'$) color cube illustrating the colors of the "cool" ULIG nuclear (2.5 kpc diameter) regions. For clarity, the ULIGs have been marked with numbers: (1) IRAS 00091−0738 (2) IRAS 01199−2307w (3,4) IRAS 03521+0028e,w (5) UGC 5101 (6,7) IRAS 12112+0305n,s (8,9) IRAS 14348−1447e,w (10) IRAS 15250+3609 (11) IRAS 20414−1651 (12,13) IRAS 22206−2715 (14,15) IRAS 22491−1448 (16,17) IRAS 23233+0946 and (18) IRAS 23365+3604. The cube is rotated to be orthogonal to the reddening vector, which is depicted by the closed boxes and represents line-of-sight extinction, i.e. a simple foreground dust screen, in units of $A_{\rm V} = 1$ magnitude. It is derived from Rieke & Lebofsky (1985). The median colors of the "warm" ULIGs are marked with a large circle. The open circles are the colors of an instantaneous starburst with a Salpeter IMF and mass range 0.1–125$M_\odot$ and aging from 0 to 15 Gyrs, based on the spectral synthesis models of Bruzual & Charlot

(1993; an updated version called BC95 is used here). The large dotted open circle is a synthetic QSO spectrum based on multiwavelength observations of Palomar-Green QSOs and is discussed in detail in Paper II. It is indicative of the colors of typical optically selected quasars. The joined, open circles show the effects of adding free-free emission with a 20,000 K electron temperature in increments of 20% of the total flux at K′ to the starburst. The two sets of filled, joined circles illustrate emission from 800 K dust contributing in increments of 10% to the total flux at K′. Finally, emission from uniformly mixed stars and dust, in units of $A_{\rm V}$=10, 30, and 50 magnitudes, are shown by the $\times$ symbol. One σ error bars are shown at upper right. Note that the line-of-sight dust extinction and thermal dust emission curves are nearly orthogonal.

Fig. 7.— Same as Figure 6, but rotated as to be parallel to the reddening vector. Error bars are at upper left.

Fig. 8.— ($B-I$),($I-H$) color-color diagram for an instantaneous starburst having a Salpeter IMF and a mass range from 0.1–125 $M_\odot$. Also shown are the colors of the star-forming knots given in Table 4.

Fig. 9.— Bolometric corrections for K-band (circles) and B-band (triangles) for an instantaneous starburst with a Salpeter IMF ranging from 0.1 to 125 $M_\odot$ (BC95).

Figures 1-5 are images and are available in JPEG format either from this preprint archive or from http://humu.ipac.caltech.edu/preprints/cool.

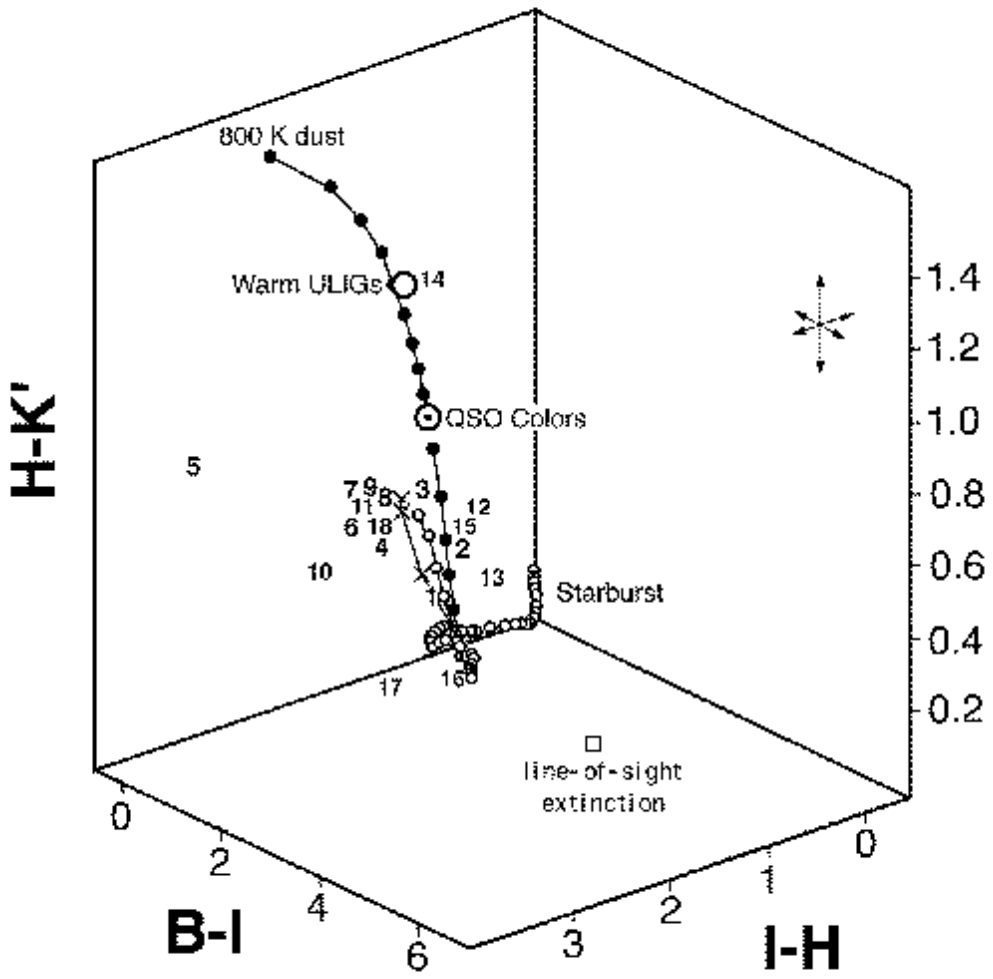
800 K dust
Warm ULIGs
14
QSO Colors
Starburst
13
12
15
2
3
5
7
9
11
8
6
18
4
10
16
17
line-of-sight
extinction
H-K'
B-I
I-H
1.4
1.2
1.0
0.8
0.6
0.4
0.2
0
2
4
6
3
2
1
0

Fig. 6.—

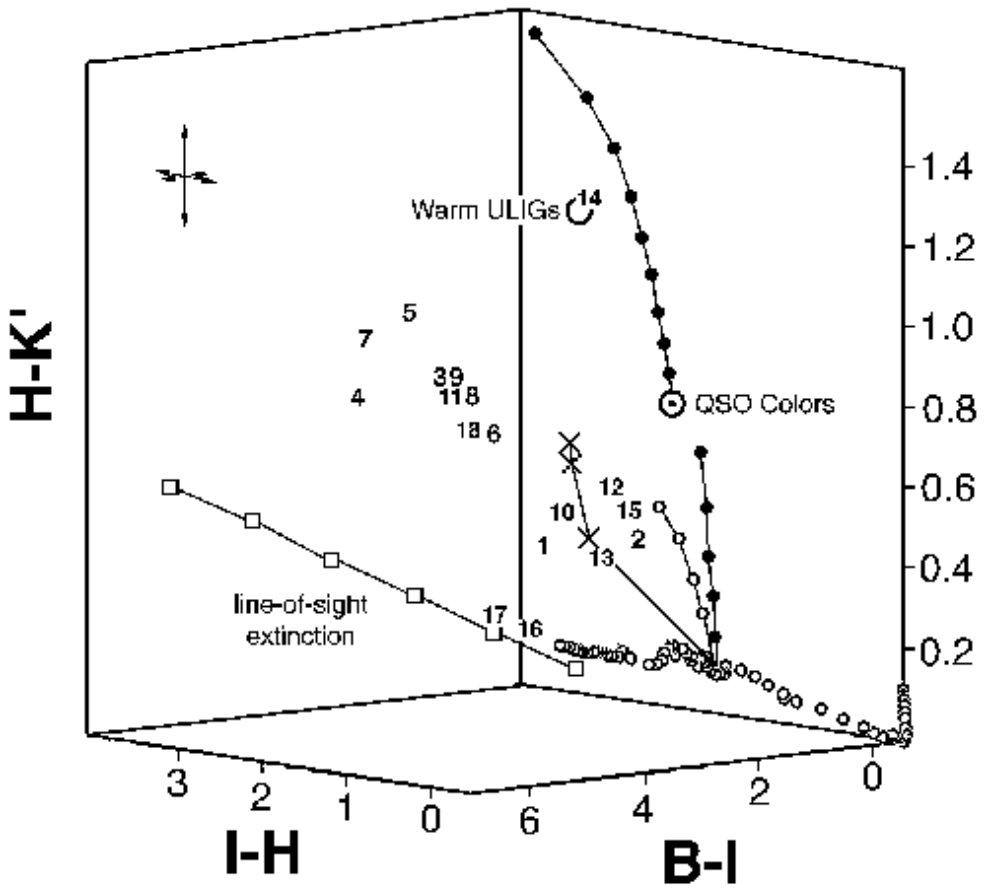
H-K'
I-H
B-I
Warm ULIGs
14
QSO Colors
line-of-sight
extinction
5
7
4
39
11
8
18
6
12
10
15
1
2
13
17
16
1.4
1.2
1.0
0.8
0.6
0.4
0.2
3
2
1
0
6
4
2
0

Fig. 7.—

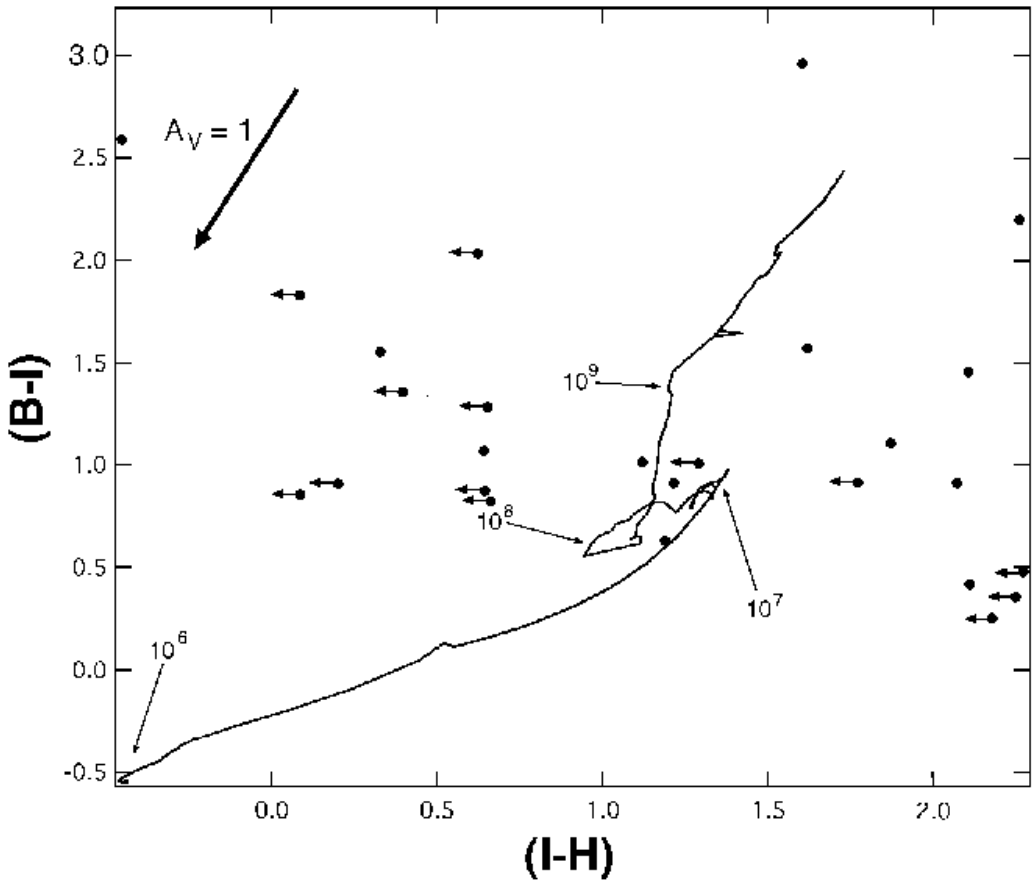

Fig. 8.—

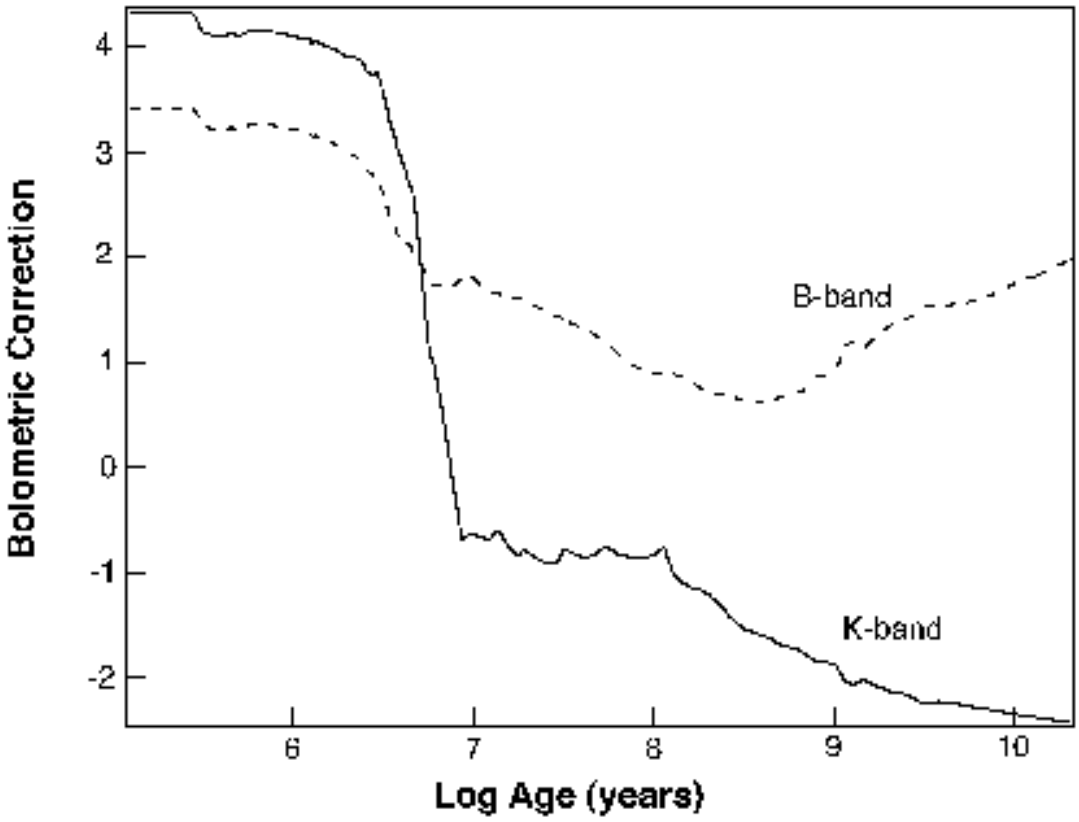
Bolometric Correction
4
3
2
1
0
-1
-2
6
7
8
9
10
Log Age (years)
B-band
K-band

Fig. 9.—

Table 1. Cool ULIG Sample & Observation Details

Name	RA[1] (J2000.0)	DEC	z	$L_{\rm ir}$ $L_\odot$	Inst.[2]	Exposure Time (sec) B	I	H	K′
IRAS 00091−0738	00:11:43.2	−07:22:07.8	0.119	12.17	QT	2520	1920	2520	1800
IRAS 01199−2307	01:22:21.4	−22:51:59.5	0.156	12.23	QT	2880	2280	2400	2160
IRAS 03521+0028	03:54:42.1	00:37:05.9	0.152	12.44	QT	3600	2280	2400	3360
UGC 5101	09:35:51.7	61:21:11.3	0.039	11.99	WQT	1620	2160	2160	2040
IRAS 12112+0305	12:13:46.1	02:48:41.4	0.072	12.24	WQT	1440	1860	1920	1440
Mrk 273	13:44:42.1	55:53:12.7	0.038	12.13	W T	1200	2340	···	···
IRAS 14348−1447	14:37:38.7	−15:00:22.8	0.082	12.24	WQH	720	720	1440	1680
IRAS 15250+3609	15:26:59.4	35:58:37.5	0.055	11.99	QH	1200	1680	2160	2160
Arp 220	15:34:57.3	23:30:11.9	0.018	12.17	NT	1080	1440	···	···
IRAS 20414−1651	20:44:17.4	−16:40:13.7	0.086	12.12	WQH	1440	1560	1680	1800
IRAS 22206−2715	22:23:28.8	−27:00:03.3	0.131	12.15	QT	480	1440	2400	2520
IRAS 22491−1808	22:51:49.3	−17:52:23.5	0.078	12.08	WQT	2520	1440	2760	2520
IRAS 23233+0946	23:25:55.6	10:02:45.1	0.128	12.02	QT	2160	1800	2160	2160
IRAS 23365+3604	23:39:01.3	36:21:09.8	0.064	12.10	QH	240	240	1200	1560

[1] Positions derived from Kim (1995), redshifts and $L_{\rm ir}$ taken from Kim (1995) and Sanders et al. (1988a)

[2] Q = UH2.2m f/31 QUIRC, T = UH2.2m f/31 Tektronix 2048, H = UH2.2m f/31 Orbit reimaged at f/10 through HARIS spectrograph, W = *HST*/WFPC2, N=*HST*/NICMOS

Table 2. Cool ULIG Morphology

Name	Nuclei[1]	Nuclear Sep. kpc	Tails[2]	Optical Knots[3]	Near-IR Knots	Spectral Class
IRAS 00091−0738	SB	···	L	Y	N	HII
IRAS 01199−2307	D	25.0	C	N	N	HII
IRAS 03521+0028	D	4.3	C	N	N	LINER
UGC 5101	SB	···	LC	Y	Y	Sy1.5
IRAS 12112+0305	SBD?	4	C	Y	Y	LINER
Mrk 273	SBD?	···	LC	Y	Y	Sy2
IRAS 14348−1447	D	5.3	L	Y	Y	LINER
IRAS 15250+3609	SC	···	C	Y	Y	LINER
Arp 220	SBD?	0.4[4]	L	Y	Y	LINER
IRAS 20414−1651	D?	2.6?	C	Y	N	HII
IRAS 22206−2715	D	9.2	L	N	N	HII
IRAS 22491−1808	D	2.5	LC	Y	Y	HII
IRAS 23233+0946	D	8.5	C	N	N	LINER
IRAS 23365+3604	SC	···	LC	Y	Y	LINER

[1] D=Double, D?=Possible Double, SC=Single Compact, SB=Single,Bifurcated

[2] L=Linear, C=Circular or semi-circular

[3] Y=Yes, N=No

[4] taken from Scoville et al. (1998)

Table 3. Cool ULIG Total and Nuclear Photometry

Name	m_B		m_I		m_H		$m_{K'}$	
	Total	Nuclear[1]	Total	Nuclear	Total	Nuclear	Total	Nuclear
IRAS 00091−0738	18.37	19.4	16.36	17.3	14.81	15.3	14.31	14.9
IRAS 01199−2307	17.82	19.5	16.69	18.0	15.11	16.2	14.85	16.2
IRAS 03521+0028	20.50	22.9	17.49	19.3	14.91	16.1	14.11	15.3
UGC 5101	14.91	17.9	14.60	16.5	11.53	12.4	10.83	11.5
IRAS 12112+0305n	16.97	20.0	15.05	18.0	12.88	15.3	12.76	14.6
IRAS 12112+0305s		21.6		18.4		15.0		14.1
Mrk 273	14.69	17.1	13.16	15.3	...	...	...	...
IRAS 14348−1447e	16.51	20.6	14.58	18.1	12.92	15.5	12.19	14.7
IRAS 14348−1447w		20.1		17.6		14.9		14.0
IRAS 15250+3609	16.17	17.5	15.19	16.6	12.98	14.0	12.77	13.6
Arp 220	14.00	17.6	12.25	14.7	10.93	11.6	10.62	10.9
IRAS 20414−1651	17.94	20.2	16.11	17.7	14.02	14.8	13.49	14.1
IRAS 22206−2715e	17.26	18.7	15.78	16.9	14.01	15.3	13.45	14.7
IRAS 22206−2715w		19.3		17.2		15.9		15.5
IRAS 22491−1808e	16.44	18.6	15.00	17.1	13.26	15.7	12.97	15.2
IRAS 22491−1808w		19.9		18.2		16.3		15.1
IRAS 23233+0946e	18.12	20.9	15.80	18.3	14.16	16.4	13.80	16.2
IRAS 23233+0946w		19.7		17.4		14.9		14.7
IRAS 23365+3604	16.17	19.5	14.32	17.1	12.68	14.5	12.19	13.8

[1] central region 2.5 kpc in diameter. Total magnitudes are listed only under the first nucleus, but refer to the entire system. Ellipses indicate missing data.

Total magnitudes are uncertain to ±0.07 magnitudes. Nuclear magnitude uncertainties are ±0.1 magnitudes.

Table 4. Star-Forming Knot Photometry

Number	ΔRA[1]	ΔDEC	$m_{\rm B}$	$m_{\rm I}$	$m_{\rm H}$	$m_{\rm K'}$
			IRAS 0009−0738			
1	1.1	0.3	21.23	19.11	> 18.50	> 18.61
			UGC 5101			
1	1.9	0.0	18.79	18.00	> 17.92	> 17.93
2	−5.6	−0.3	20.24	20.04	> 17.63	> 18.66
3	−4.6	0.7	20.03	19.85	> 17.63	> 18.66
4	−3.8	2.9	20.42	20.03	> 17.63	> 18.66
5	9.4	1.4	20.61	20.27	> 17.90	> 19.00
6	6.3	10.0	21.63	20.15	18.07	18.03
			IRAS 12112+0305			
1	−2.8	0.3	20.32	18.22	15.92	15.53
2	−2.7	−2.8	21.62	18.37	15.09	14.33
3	−2.8	−7.4	19.90	18.31	16.69	16.32
			Mrk 273			
1	−0.7	−3.64	17.61	16.09	···	···
			IRAS 14348−1447			
1	−1.1	1.3	19.31	18.42	> 17.75	> 17.17
2	−1.3	−1.4	19.69	18.42	> 17.75	> 17.17
3	3.2	4.1	19.12	18.25	> 18.00	> 17.03
			IRAS 15250+3609			
1	0.5	−0.4	···	···	14.39	13.96
2	1.5	1.4	20.50	17.86	18.50	18.33
3	−0.5	1.1	19.33	18.21	17.07	16.53
4	−2.0	0.7	20.18	19.61	18.43	18.13

Table 4—Continued

Number	ΔRA[1]	ΔDEC	$m_{\rm B}$	$m_{\rm I}$	$m_{\rm H}$	$m_{\rm K'}$
5	−0.3	−1.1	19.97	18.74	16.88	16.55
IRAS 20414−1651						
1	1.8	1.1	19.86	18.21	17.86	17.18
2	−3.8	−9.0	20.69	19.76	> 18.40	> 18.13
IRAS 22491−1808						
1	0.0	1.0	21.44	18.46	16.98	16.65
2	−2.5	1.1	19.79	19.38	17.18	16.73
3	−3.2	1.5	20.35	19.38	17.19	16.73
4	−1.0	−0.6	19.07	18.00	16.92	> 17.19
5	0.4	−1.1	20.28	19.11	18.56	> 17.76
IRAS 23365+3604						
1	−1.9	1.4	19.93	18.45	> 18.00	> 17.65
2	2.2	1.3	21.55	20.62	> 18.88	> 18.69
3	1.4	−2.4	20.29	19.57	> 18.88	> 18.25
4	−0.3	−1.5	19.70	17.84	> 17.80	> 17.32

[1] RA and DEC offsets measured from the centroid of the "nucleus", i.e., the brightest emission source at I-band

Reference to the knots should be made in accordance with the I AU naming convention (galaxy name):SS(number).

This figure "fig1.jpg" is available in "jpg" format from:

http://arXiv.org/ps/astro-ph/9909085v1

This figure "fig1b.jpg" is available in "jpg" format from:

http://arXiv.org/ps/astro-ph/9909085v1

This figure "fig1c.jpg" is available in "jpg" format from:

http://arXiv.org/ps/astro-ph/9909085v1

This figure "fig2.jpg" is available in "jpg" format from:

http://arXiv.org/ps/astro-ph/9909085v1

This figure "fig3.jpg" is available in "jpg" format from:

http://arXiv.org/ps/astro-ph/9909085v1

This figure "fig4.jpg" is available in "jpg" format from:

http://arXiv.org/ps/astro-ph/9909085v1

This figure "fig5.jpg" is available in "jpg" format from:

http://arXiv.org/ps/astro-ph/9909085v1

This figure "fig5b.jpg" is available in "jpg" format from:

http://arXiv.org/ps/astro-ph/9909085v1